International Journal of Biological Macromolecules 193 (2021) 1823–1834

Contents lists available at ScienceDirect

International Journal of Biological Macromolecules

journal homepage: www.elsevier.com/locate/ijbiomac

# Preparation and characterization of succinyl chitosan and succinyl chitosan nanoparticle film: *In vitro* and *in vivo* evaluation of wound healing activity

N.T. Thu Thao [a], H.M.S.M. Wijerathna [b], R. Saravana Kumar [c], Dongrack Choi [a], S.H. S. Dananjaya [a,*], A.P. Attanayake [d,*]

[a] Zerone Bio Inc., Dankook University, 3rd Floor, Sanhak Building, Dandae-ro 119, Dongnam-gu, Cheonan Si, Chungcheongnam-do 31116, Republic of Korea
[b] Department of Aquaculture and Aquatic Resources Management, University College of Anuradhapura, Sri Lanka
[c] Department of Physics, Government College of Arts and Science, Idappadi, Salem 637102, Tamil Nadu, India
[d] Department of Biochemistry, Faculty of Medicine, University of Ruhuna, Galle, Sri Lanka

ARTICLE INFO

*Keywords:*
*N*-succinyl chitosan
Nanoparticles
*N*-succinyl chitosan film
Cytotoxicity
Wistar rats
Wound healing

ABSTRACT

Development of novel wound dressing materials having the ability to prevent bacterial infections and capable of accelerating the tissue regeneration process is utmost important, since the wounds in patients can cause severe health issues. In the present work, we synthesized novel *N*-succinyl chitosan nanoparticles (*N*-SuC NPs) films and tested their antimicrobial, cytotoxicity, and *in vitro* and *in vivo* wound healing activity. *N*-SuC NPs were synthesized by ionic gelation method, and subsequently *N*-SuC NPs films were prepared by solution casting method using synthesized *N*-SuC NPs. The prepared *N*-SuC NPs films showed significant antimicrobial activity against *Escherichia coli* and *Staphylococcus aureus* with a minimum inhibitory concentration of 6 mg/mL and <8 mg/mL, respectively. The biocompatibility and the *in vitro* wound healing activity of *N*-SuC NPs films were analyzed using human dermal fibroblast (HDF) cells. *In vivo* cutaneous wound healing of the *N*-SuC NPs film was investigated using the Wister rat model, and the studies showed that the *N*-SuC NPs film significantly accelerated the wound healing process by inducing more blood vessels formation and tissue granulation. The experimental results showed that synthesized *N*-SuC NPs film had excellent antimicrobial, cytotoxicity and wound healing activity, indicating that it could be used in biomedical applications.

## 1. Introduction

Non healing wounds cause severe pain to patients and present substantial financial issues for those affected. A chronic or acute wound is created when there is a disruption in the integrity of skin or organ tissue [1]. Normally, skin tissues have the ability to self-heal and regenerate themselves in case of minor injuries such as cuts and abrasions. However, in non-trivial injuries or in combinations with additional complications such as diabetes mellitus, chronic ulcers, healing capacity is greatly reduced and becomes a complex process [2]. The costs incurred by chronic non-healing wounds would place a massive financial strain on the world's healthcare systems [3]. Wound healing is a highly complex and coordinated repair process that takes place in a series of overlapping phases. The natural wound healing process includes conventional overlapping steps known as hemostasis, inflammation, proliferation, and remodeling [4,5]. Furthermore, the timing of wound healing is critical to initiate tissue regeneration without abnormalities [6]. Hence, several studies were conducted to develop wound dressings using natural polysaccharides such as chitin, chitosan, alginate, sodium hyaluronic, glucan and pectin [7–9]. The wound dressings are not only capable of preventing bacterial infection, but also maintain a moist environment in the wound, absorbing excessive extrudate, and accelerating the tissue regeneration process [10,11]. Hence, it is utmost important to develop novel wound dressings that have the potential to shorten the anti-inflammatory phase and accelerate cell proliferation.

Chitosan possesses exceptional properties as a cationic polysaccharide, including biodegradability, biocompatibility, non-toxicity, antimicrobial activity and hemostatic properties [2,12]. Furthermore, it has a high capacity to absorb large amounts of fluids, which allows the wound environment to remain moist, which is an important feature of any dressing material [13]. In addition, chitosan exhibits excellent ability to form a film with good mechanical properties and antimicrobial activities [14]. Due to the aforementioned properties of chitosan, it is a potential candidate for medical applications such as wound dressing and

* Corresponding authors.
*E-mail addresses:* sajith@zeronebio.com (S.H.S. Dananjaya), anojaattanayake@med.ruh.ac.lk (A.P. Attanayake).

https://doi.org/10.1016/j.ijbiomac.2021.11.015
Received 16 May 2021; Received in revised form 22 October 2021; Accepted 2 November 2021
Available online 13 November 2021

tissue engineering, as well as for industrial applications such as food packaging [15]. However, the structure of chitosan results in poor water solubility. As a result, hydrophilic groups are typically introduced by chemical modification to improve chitosan solubility and broaden its potential applications. The introduction of succinyl groups into the glucosamine units of the chitosan *N*-terminal improves the solubility of chitosan. *N*-succinyl chitosan (*N*-SuC) has been reported as a wound healing accelerator [16] due to its incredible adsorbent, adhesion [17,18], and other favorable biochemical properties [19,20]. The wound healing properties of *N*-SuC can be improved by synthesizing *N*-SuC in nanoparticles (NPs) form. *N*-SuC NPs can be synthesized through ionic gelation caused by the inter- and intra-molecular cross-linking of protonated amino groups in *N*-succinyl chitosan by multivalent polyanions [21]. The *N*-SuC NPs are environmentally friendly materials with excellent physicochemical properties, and are known to have many applications in the field of gene carrier and drug delivery [20–24]. Several studies have been conducted to develop food packaging using bio-nanocomposite films with antibacterial and biodegradable properties by incorporating chitosan NPs into polymeric matrices such as cellulose, starch, and gelatin [25–28]. On the other hand, the wound healing activity of *N*-SuC and *N*-SuC NPs films has yet to be reported.

Hence, in this study, we synthesized *N*-SuC and *N*-SuC NPs by the ionic gelation method, and then prepared the corresponding films using the solution casting method. The synthesized *N*-SuC and *N*-SuC NPs films were characterized according to their physicochemical and mechanical properties. The antimicrobial activity of the *N*-SuC and *N*-SuC NPs films was investigated against *Escherichia coli* (gram-negative) and *Staphylococcus aureus* (gram-positive), two of the most commonly observed foodborne bacteria. The biocompatibility and *in vitro* wound healing activity of *N*-SuC and *N*-SuC NPs films were analyzed using human dermal fibroblast (HDF) cells. In addition, the *in vivo* cutaneous wound healing activity of *N*-SuC and *N*-SuC NPs were investigated using the Wistar rat model.

## 2. Experimental details

### 2.1. Preparation and characterization of N-SuC

*N*-SuC was prepared according to the previously reported procedure using crab shell chitosan (Shaanxi Boling Biotechnology Co., Ltd., China) with a average molecular weight ($6.7 \times 10^4$ Da) and a degree of deacetylation %(DD); 73% (potentiometric titration), 69% ($^1$H NMR)] [18]. Briefly, 5 g of chitosan was dissolved in 200 mL of 3% (*v*/v) acetic acid solution (Sigma Aldrich, USA), followed by addition of 400 mL of methanol to dilute the solution. Then, 12 g of succinic anhydride (Junsei Chemical Co., Ltd., Japan) was added to the above solution at room temperature under constant stirring, and the reaction mixture was continuously stirred at room temperature for 12 h. *N*-SuC was isolated using the precipitation technique by adjusting the pH of the chitosan mixture solution to ~6–7. The resultant *N*-SuC white precipitate was further washed with ethanol to remove the unreacted chemicals, filtered, and dissolved in distilled water. The pH was then adjusted to 10 and the solution was dialyzed for three days through 8000–10,000 Da molecular weight cut-off dialysis tub, and freeze-dried to obtain the purified *N*-SuC. The obtained pure *N*-SuC polymer was stored at −4 °C until use.

X-ray diffraction (XRD) analysis was carried out using Bruker D8-Advance X-ray diffractometer (USA) with Cu Kα radiation (λ = 1.544 Å). Fourier transform infrared spectra (FTIR, Shimadzu, Japan) were obtained by recording 50 scans between 4000 and 400 $cm^{-1}$ with a resolution of 2 $cm^{-1}$. The degree of deacetylation of chitosan was determined by potentiometric titration according to a previously described method [29]. Briefly, chitosan (~0.05 g) was dissolved in an excess aqueous acidic solution (0.1 M HCl solution), and the solution was then titrated with 0.1 M NaOH measuring pH (OHAUS-ST3100). The degree of deacetylation (% *DD*) was calculated using the formula:

$$DD = 161\ X\ 10^{-3} X\ (y - x)\left(\frac{M}{W}\right) X100$$

where, 161 is the molar mass of the monomeric unit of fully deacetylated chitosan (g $mol^{-1}$), 'x' and 'y' are the first and second equivalent points (mL), respectively, and '*M*' is the concentration of NaOH solution (mol $L^{-1}$), and '*w*' is the weight of the chitosan (g).

In addition, the percentage degree of acetylation (DA) was then calculated from the integrals of the $^1$H NMR spectrums using the following equation: $DA = \left[\left(\frac{\delta\ CH3=O}{\delta\ H2-H6)}\right)\left(\frac{6}{3}\right)\right] X100$. Average of DA values from two measurements was taken as the final value. DD was obtained by calculating % DD = (1-DA)*100. The chemical structure of chitosan and *N*-SuC was analyzed by a JEOL ECA 400 nuclear magnetic resonance (NMR) equipped with Delta™ analytical software in order to determine the average values of succinyl groups substituted at the *N*-positions along the chitosan chains. The 2% *v*/v $CD_3COOD/D_2O$ was used as the solvent to dissolve chitosan and *N*-SuC, and tetramethylsilane (TMS) was used as the internal standard (0.0 ppm). The ratio of $CH_2CH_2$ of succinyl peak intensity to that of the C2 (H-2 of d-glucosamine unit ~3.00 ppm) proton of chitosan was taken to calculate degree of substitution (DS). The degree of substitution (DS) of *N*-SuC was calculated according to the following equation, $DS = \frac{\delta\ A/4}{\delta\ B/1} X\ 100$ [30].

High Performance size exclusion chromatography (HPLC-Agilent 1100, USA) was used to determine the molecular weight of the chitosan and *N*-SuC. First, the prepared solutions of chitosan and the *N*-SuC products were diluted with buffer solution of acetic acid (0.40 M) /sodium acetate (0.20 M) to obtain the solutions at a fixed concentration of 0.1 wt% (final pH of the solutions - 3.5). Each of the sample solutions (100 μL) was injected into the high performance size exclusion chromatography equipment which was equipped with a Shodex SB-804HQ, SB-806HQ OHpak column (Showa Denko, Japan) at 55 °C using a reflective index (RI) detector. The flow medium was buffer solution of acetic acid (0.20 M) /sodium acetate (0.10 M) and the flow rate was 0.6 mL/min. Standard pullulan kit P82 were used in the calibration.

### 2.2. Preparation and characterization of N-SuC NPs and N-SuC NPs films

***Synthesis of N-SuC NPs:*** *N*-SuC NPs were prepared according to the method reported previously [31], with minor modifications. Initially, 4 mg/mL of *N*-SuC and 0.8 mg/mL of sodium tripolyphosphate (TPP, Junsei chemical Co., Ltd., Japan) were dissolved in deionized water and the pH of the *N*-SuC solution was adjusted to 6.0 by adding acetic acid (3.0 M). The *N*-SuC NPs were formed spontaneously by adding 10 mL of TPP aqueous basic solution to 10 mL *N*-SuC solution under constant stirring for 30 min at room temperature. Subsequently, purified *N*-SuC NPs were obtained by ultracentrifugation (20,000 rpm, 1 h, 4 °C). The obtained *N*-SuC NPs were redispersed in water.

***Preparation of N-SuC and N-SuC NPs films:*** For the preparation of the *N*-SuC film, 0.4 g of *N*-SuC was dissolved in 100 mL of distilled water. Glycerol was used as a plasticizer at 15% (% w/w of polymer). The *N*-SuC NPs film was prepared using 100 mL *N*-SuC NPs suspension with glycerol. The mixture of *N*-SuC and *N*-SuC NPs was vigorously stirred and stored at 4 °C for one day to remove air bubbles. The resulting solution was casted in a 9 cm diameter petri dish and dried at 50 °C for 24 h. To maintain constant moisture content, *N*-SuC and *N*-SuC NPs films were stored in a vacuum desiccator at 10 °C.

***Characterization of N-SuC and N-SuC NPs films:*** The particle size, polydispersity index (PDI) and the zeta potential of *N*-SuC NPs suspension (1 mg/mL, pH ~6.0) were analyzed using a Zetasizer Nano-ZS (Malvern Instruments, UK) on the basis of dynamic light scattering (DLS) techniques. The measurements were performed at a temperature of 25 °C in triplicate. The morphology of *N*-SuC NPs was examined using high-performance digital imaging Transmission Electron Microscopy (TEM, JEOL 2100, Hitachi High-Technologies Corp., Japan). Dynamic

rheological measurements of *N*-SuC and *N*-SuC NPs films forming solution were conducted using a rheometer (MCR 102 Anton Paar). The storage modulus ($G'$) and loss modulus ($G''$) were measured as a function of frequency from 0.1 to 100 Hz at a constant strain of 0.1%. The thicknesses of the *N*-SuC and *N*-SuC NPs films were measured using a handheld digital micrometer (Mitutoyo Manufacturing Co. Ltd., Tokyo, Japan) with a sensitivity of 0.001 mm. Thickness measurements were taken at five different locations in each film (center and four corners), and the mean thickness value was calculated. The mechanical characteristics such as tensile strength and the elongation at break were measured using a Universal Testing Machine (Instron Corp, Watertown, MA, USA) fitted with a 0.01 kN load cell. Films were cut into 100 mm × 15 mm rectangular dimensions, and stretched at 10 mmmin$^{-1}$ from 50 mm initial gap until breakage. During the mechanical assay, the relative humidity and temperature did not exceed 60% and 27 °C, respectively. The tensile strength was calculated by dividing the maximum tensile stress by the cross-sectional area of the specimens, and the elongation at break was calculated by dividing the sample length at breakage by its initial length (50 mm). The surface morphology of *N*-SuC and *N*-SuC NPs films (0.5 × 0.5 cm$^2$) was examined using a field emission scanning electron microscope (FESEM, SEISS, Germany) with an accelerating voltage of 5 kV at different magnifications (10, 100 and 200 k). The surface roughness of *N*-SuC and *N*-SuC NPs films was further analyzed using Atomic Force Microscopy (AFM, Bruker Dimension Icon, Bruker Co., Germany). Samples were scanned in non-contact modes using a sharpened cantilever with a spring constant of 25 N/m, and 5 μm × 5 μm images were obtained. To calculate the roughness values, all samples were analyzed in triplicate using Bruker Nanoscope analysis software (Version 1.40). The parameters such as arithmetic average height ($R_a$), which is the arithmetic average height parameter of the absolute values of the surface height deviations ($Z$) measured from the mean plane, and the root mean square average ($R_q$) which is the root mean square average of height deviations taken from the mean image data plane were calculated.

### 2.3. In vitro antibacterial and biofilm inhibition effect of N-SuC and N-SuC NPs films

The minimal inhibitory concentrations (MIC) of *N*-SuC and *N*-SuC NPs films against *Staphylococcus aureus* (*S. aureus*, KCTC 1916) and *Escherichia coli* (*E. coli*, ATCC25922) were determined using the micro dilution method. For the liquid growth inhibition assay, overnight cultures of *S. aureus* and *E.coli* were inoculated in a 20 mL fresh culture media at 1:100 dilution (1.0 × 10$^5$ CFUmL$^{-1}$), and then different concentrations of *N*-SuC and *N*- SuC NPs films (ranging from 500 to 8000 μg/mL) were added to the broth and incubated at 37 °C. The lowest concentration of *N*-SuC or *N*-SuC NPs film that inhibits the visible growth was considered as the MIC. After 48 h of incubation, the optical density (OD) value of each mixture was estimated at 610 nm. The bacterial inhibition ratio of *N*-SuC or *N*-SuC NPs film at various concentrations was calculated after 48 h using the following Eq. [16]:

$$\text{Inhibition ratio (\%)} = 100–100 \times [(A_t - A_0)/(A_{ctrl} - A_0)].$$

where, '$A_0$' is the OD value of the bacterial broth medium before incubation. '$A_t$' and '$A_{ctrl}$' are the OD values of the film and the control group at different incubation times, respectively.

The biofilm inhibition activities of the *N*-SuC and *N*-SuC NPs films against *S. aureus* and *E. coli* were quantified using a crystal violet assay [32]. Overnight cultures of *S. aureus* and *E. coli* were cultured separately in Luria Bertani broth and were adjusted to obtain a final concentration of ~3 × 10$^6$ CFU/mL. The 90 μL of *S. aureus* and *E. coli* culture (3 × 10$^6$ CFU/mL) was placed in a 96-well plate and treated with 10 μL of eluted films elute to reach different concentrations of *N*-SuC and *N*-SuC NPs (500–8000 μg/mL), and incubated for 24 h at 37 °C. After 24 h post-treatment (hpt), supernatants were removed by pipetting. The biofilm was then washed with PBS and fixed with 100 μL of absolute methanol for 10 min. After removing the methanol, the attached biofilm was stained with 0.1% (*w/v*) crystal violet (Sigma-Aldrich, USA) for 30 min at room temperature. The crystal violet was then removed by pipetting, and the biofilm was washed with PBS. Finally, the stained biofilm was dissolved in ethanol (95%) and the absorbance was measured at 595 nm using a microplate reader (Bio-Rad, USA). The percentages of biofilm inhibition were calculated using the following formula: biofilm formation inhibition % = [1 – ($Ab_{test}$/$Ab_{negative\ control}$)] × 100%, where '$Ab_{test}$' represents the absorbance value of *N*-SuC and *N*-SuC NPs, and '$Ab_{negative\ control}$' represents the absorbance of the negative control (PBS).

### 2.4. In vitro cell proliferation effect of N-SuC and N-SuC NPs films

Human dermal fibroblast (HDF) cells were purchased from the American Type Culture Collection (Normal, Human, Adult (ATCC® PCS-201-012™) and cultured in Dulbecco's modified Eagles medium (DMEM) (Hyclone, GE Healthcare Life Sciences, USA), supplemented with 1% antibiotic-antimycotic (Gibco, USA) and 2% fetal bovine serum (FBS, Hyclone, Fisher Scientific, USA). Cell proliferation of *N*-SuC and *N*-SuC NPs films was evaluated using the WST-1 assay (Roche) according to the manufacturer's instructions. The *N*-SuC and *N*-SuC NPs films were UV-sterilized for 30 min before different weights of the films were immersed in 5 mL of serum-containing medium (0.1 to 1.2 mg/mL) for 24 h at 37 °C.

In brief, HDFs were seeded at an initial concentration of 3 × 10$^3$ cells/well in a 96 well plate and pre-cultured with 200 μL culture medium for 24 h. The cells were then treated with different concentrations of *N*-SuC and *N*-SuC NPs films supernatants. Untreated cells were used as controls. The plates were then incubated for 48 h before the WST-1 assay was performed. Following the incubation period, the medium was removed and 150 μL of medium containing 10% WST-1 solution was added to each well. After 30 min of incubation, 100 μL of this medium was transferred to a 96-well plate and OD was measured at 450 nm using a microplate reader (BIO-TEK, Senergy HT) with fresh media as blank for quantitative analysis. The percent viability of the cells was expressed as a ratio of treated cells to control cells. To evaluate the cytotoxicity of *N*-SuC and *N*-SuC NPs films elutes, we performed a live/dead staining (LIVE/DEAD™ Viability/Cytotoxicity Kit, for mammalian cells, Invitrogen™, CA, USA). After incubating the cells with 600 and 1200 μg/mL of *N*-SuC and *N*-SuC NPs films elutes, we treated each well with a 100 μL mixture of 4 mM calcein (calcein AM, Component A) and 2 mM ethidium homodimer-1 (Component B), and incubated the cells at 37 °C for 15 min. After incubation, the stained cells were observed using a Nikon Eclipse Ti-E fluorescence microscope (Tokyo, Japan).

The cell morphology of *N*-SuC and *N*-SuC NPs films (600 and 1200 μg/mL) elutes treated cells was visualized at 48 hpt using a fluorescence microscopy. 4′,6-Diamidino-2-phenylindole dihydrochloride (DAPI, 1 μg/mL) and PhalloidinTetramethylrhodamine B isothiocyanate staining (Phalloidin-TRITC, 1 μg/mL, Sigma, USA) were used to stain the cell nucleus and actin-cytoskeleton, respectively. Briefly, cells were washed with PBS and fixed with 4% paraformaldehyde for 15 min, followed by treatment with 0.5% Triton-X for 10 min to permeabilize the cell membrane. After the staining with Phalloidin (for 25 min) followed by DAPI (10 min) cells were washed with PBS. Images were captured using a Nikon Eclipse Ti-E fluorescence microscope (Tokyo, Japan).

### 2.5. In vitro wound healing activity of N-SuC and N- SuC NPs films

The *in vitro* wound healing activity of *N*-SuC and *N*-SuC NPs films was evaluated using a culture-insert (μ-Dish 35 mm, ibidi, Munich, Germany) composed of two reservoirs separated by a distance of 500 μm. For the HDF migration assay, 70 μL of cell suspension (5 × 10$^5$ cells/mL) was placed in each well and incubated at 37 °C (with 5% $CO_2$). After 24 h the cells were attached and spread to form a confluent monolayer and the insert was gently removed, creating a cell-free gap (500 μm) resembling wound creation. The μ-Dish was then filled with 2 mL of elutes from the *N*-SuC and *N*-SuC NPs films. The FBS free medium was

used as the control. Images of the cell-free gap were taken at 0, 12, 24, and 36 h using an inverted light microscope (Leica® DMi8, Germany) to determine the time required for the cell migration to fill the cell-free gap. The experiments were performed in triplicate ($n = 3$) and the cell-free gaps were analyzed using ImageJ software (ImageJ, ver. 1.6, USA) by normalizing to the 0 h cell-free gap.

### 2.6. In vivo wound healing activity of N-SuC and N-SuC NPs films

The ethical clearance for the *in vivo* wound healing study was granted by the Ethical Review Committee of Faculty of Medicine, University of Ruhuna, Sri Lanka (2021.P.010). The wound healing experiments in Wistar rats were performed at the Animal Research Facility Center, Department of Biochemistry, Faculty of Medicine, University of Ruhuna, Sri Lanka, according to the 3R principle, adhering to a framework for carrying out animal research. Animals were housed in pairs in stainless rat cages, water and standard food pellets were provided *ad libitum*. They were maintained under standard laboratory conditions and allowed for 14 days of acclimatization prior to the commencing of experiments. The minimum required number of animals was allocated to an experimental group. All experiments were conducted in a local exhaust ventilation system. Safety glasses, lab coat, compatible chemical resistant gloves (nitrile gloves) *etc.* were used in handling chemicals and tissue samples.

Eight weeks old male Wister rats (180 ± 20 g) were anesthetized by intra-peritoneal (i.p.) injection of ketamine (50 mg/kg) + xylazine (5 mg/kg). Rats were shaved and wound sites were sterilized with 70% ethanol and povidine. Wound defects were created using an 8 mm biopsy punch on the back of the rat. Each rat carried two defects and the wounded rats were randomly divided into three groups based on the body weight of animals (twelve in each group) namely group 1, group 2 and group 3 treated with control, *N*-SuC film and *N*-SuC NPs film, respectively. After the wound was created, an 8 mm diameter *N*-SuC and *N*-SuC NPs films sheet was inserted into the wound and covered with a sterilized cotton dressing (reapplied every 2 days for the first week). Digital photographs were taken on the 0, 3$^{rd}$, 7$^{th}$, 10$^{th}$ and 14$^{th}$ day of the post-procedures to assess the healing process. The wounded area was measured using ImageJ software (ImageJ, ver. 1.6, USA). The percentage of wound closure rate was estimated using the following Eq. [16]: (origin wound area - residual wound area on day 'X') / origin wound area×100%).

The animals were euthanized by overdose of thiopentone injection (ip). The wound site tissue was collected on the 3$^{rd}$, 7$^{th}$, 10$^{th}$ and 14$^{th}$ day, and fixed in a 10% formalin solution. Following the 12 h washing step, tissues were dehydrated by passing through an ascending graded series of alcohol and cleared with xylene in a Semi-enclosed Benchtop Tissue Processor (Leica® TP1020, Germany). Subsequently the tissues were embedded in paraffin wax (Leica® EG1150 Tissue Embedding Center, Germany) and sectioned (Leica® RM2125 microtome, Germany). To study the morphology of wound site, 5 μm thick sections were stained with hematoxylin and eosin (H & E). Finally, the stained tissues from each group were imaged on 10 randomly selected fields using a Nikon eclipse 80i (Nikon Corporation, Tokyo, Japan).

### 2.7. Statistical analysis

The values are given as mean ± standard deviations (SD) of the number of experiments ($n = 6$). Statistical analyzes were performed using GraphPad Prism software (GraphPad Software, CA, USA). Statistical significance was determined by *t*-test analysis with $p < 0.05$ considered as statistically significant.

## 3. Results and discussion

### 3.1. Characterization of N-SuC

The $^1$H NMR, XRD and FTIR spectra of chitosan and *N*-SuC are given in Fig. 1. The succinylation reaction was confirmed by the condensation between the amino group of chitosan backbone and the electrophilic carbonyl groups of succinic anhydride, resulting in an amidic bond with anhydride ring opening [33]. The $^1$H NMR assignments of *N*-SuC were as follows: $^1$H NMR (deuterium [$D_2O$]) $\delta$ =1.94 ppm (NH[*CO*]$CH_3$); $\delta$ =2.53 ppm ($CH_2CH_2$ of succinyl); $\delta$ =3.06 ppm (H-2 of d-glucosamine unit); $\delta$ =3.60–3.78 ppm (H-3, H-4, H-5, H-6, H-6′ of d-glucosamine unit), and $\delta$ =4.71 ppm (H-1 of d-glucosamine unit). The $^1$H NMR spectral data of the synthesized *N*-SuC were identical to those reported previously [34,35]. The DS of the succinyl group during the reaction was found to be 9 ± 3%. The % DD of N-SuC was found to be 56% ($^1$H NMR). The DS of succinyl groups had no relation with the DD value of chitosan. The substitution of the succinyl groups on the chitosan chains mainly

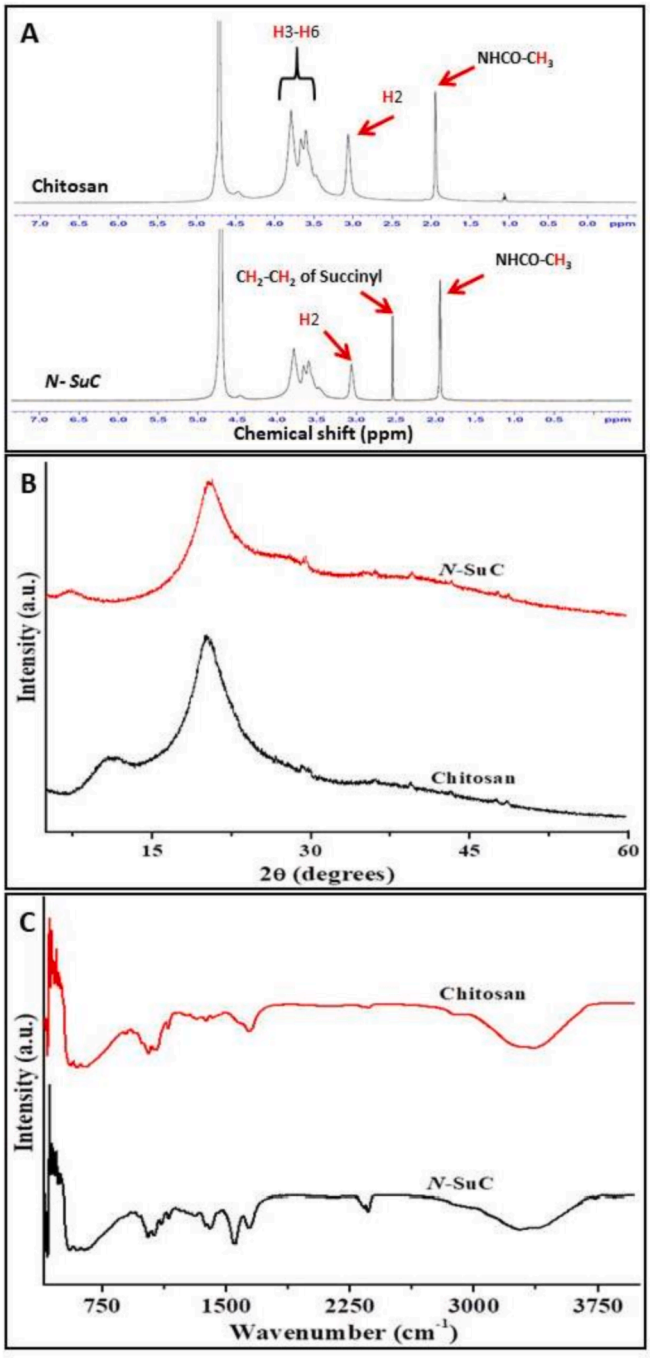


**Fig. 1.** (A) $^1$H NMR spectra, (B) XRD spectra, and (C) FTIR spectrum of chitosan and *N*-SuC.

depend on the succinic anhydride to $NH_2$ ratio and reaction time.

The XRD spectra of chitosan showed characteristic diffraction peaks at $2\theta = 10.55°$ and 19.98°, whereas the XRD spectra of *N*-SuC showed a less intense and broad diffraction peak at $2\theta = 19.86°$, and the diffraction peak at 10.55° disappeared (Fig. 1B). The presence of strong intermolecular and intramolecular hydrogen bonds (*H*-bonds) causes chitosan to be crystalline [36]. The intermolecular H-bonds in chitosan are greatly reduced during the formation of *N*-SuC due to the successful substitution of succinyl group into the chitosan backbone [36]. This weak intermolecular *H*-bond in *N*-SuC might help to increase their solubility in water. The FTIR spectra of chitosan and *N*-SuC showed a similar spectral profile with slight variation in the characteristic absorption bands (Fig. 1C). The chitosan spectrum showed the distinctive absorption bands at 1381 $cm^{-1}$ (C—H bending), 1650 $cm^{-1}$ (C═O stretching), 1599 $cm^{-1}$ (N—H bending), and 3358 $cm^{-1}$ (-OH and -$NH_2$ combined stretching). The absorption bands at 1149 $cm^{-1}$ (C-O-C asymmetric stretching) and 1029 $cm^{-1}$ (skeletal vibration involving the C—O stretching) are the characteristic absorption bands of chitosan saccharine structure in *N*-SuC. On the other hand, in the FTIR spectrum of *N*-SuC the absorption band of -OH and -$NH_2$ combined stretching (3331 $cm^{-1}$) becomes broader and shifts to a lower wave number. The FTIR spectrum of *N*-SuC also showed new absorption bands at 1404 $cm^{-1}$ corresponding to the symmetric stretching vibrations of COO- ions, and 1552 $cm^{-1}$ corresponding to the symmetric stretching of the

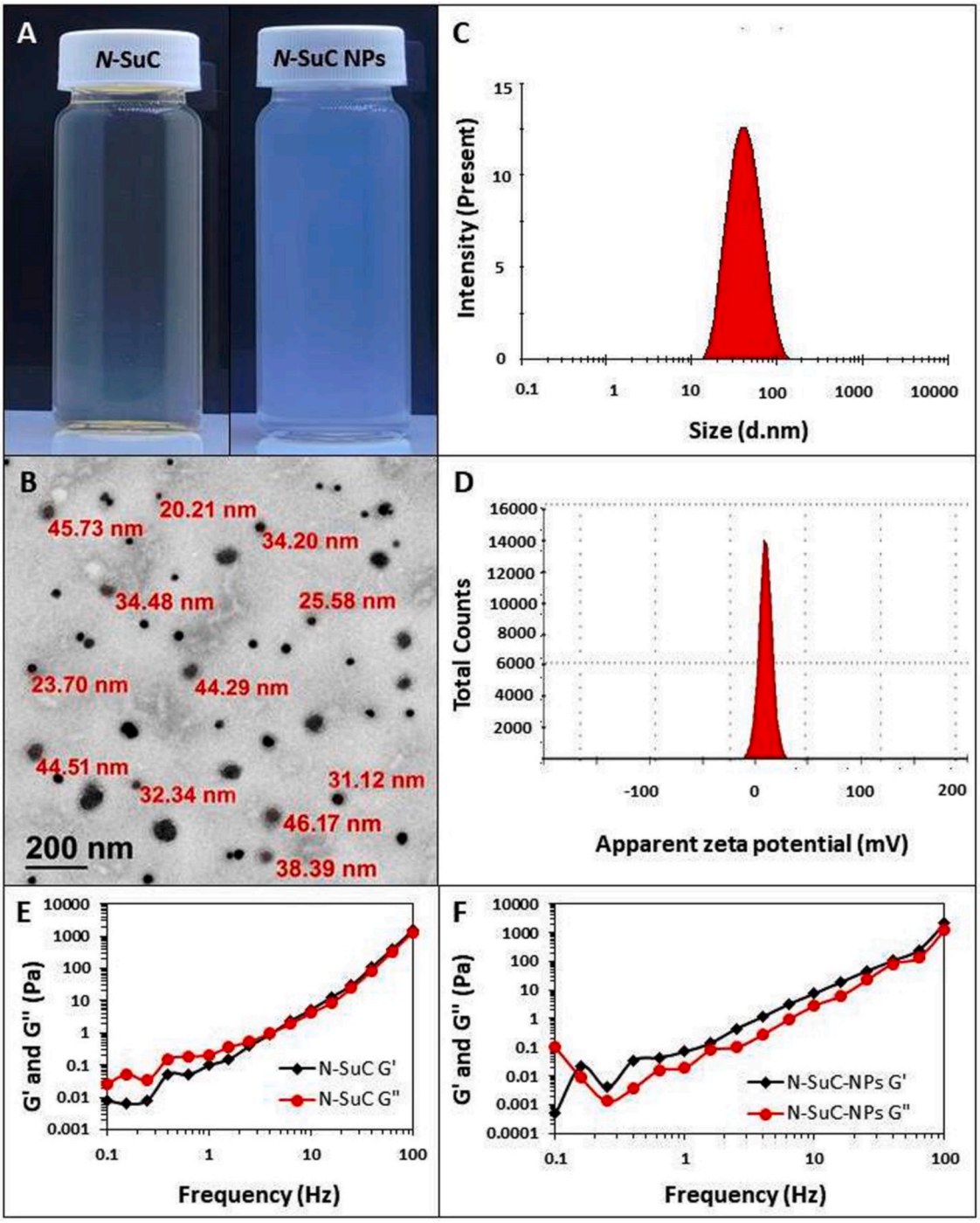


**Fig. 2.** (A) Photographic image of *N*-SuC and *N*-SuC NPs aqueous solutions; and (B) FE TEM, (C) Average particle size distribution profile, and (D) Zeta potential distribution profile of *N*-SuC NPs; (E and F) Frequency dependence of storage (G′) and loss (G″) modulus of *N*-SuC and *N*-SuC NPs film-forming solutions.

-COOH group. This new absorption bands in *N*-SuC provides the direct evidence for the successful modification of chitosan with succinic anhydride. The FTIR spectral data of the synthesized *N*-SuC were identical to those reported previously [37,38]. After succinylation, the average molecular weight of chitosan increased from $6.7 \times 10^4$ to $10.3 \times 10^4$ Da.

### 3.2. Characterization of N-SuC NPs

The *N*-SuC NPs were prepared by ionic gelation method through the electrostatic interaction between the positively charged amine group ($-NH_3^+$) of *N*-SuC and the negatively charged phosphate groups ($-P_3O_{10}^{5-}$) of TPP. Hassani et al. [39], pointed out that the increase in the turbidity of the solution indicates the formation of chitosan-sodium tripolyphosphate (TPP) NPs. The change in color (opaque color) of *N*-SuC solution confirmed the formation of *N*-SuC NPs suspension (Fig. 2A). The TEM image of *N*-SuC NPs showed nearly spherical shaped NPs with an average diameter of 30 nm (Fig. 2B). The average particle size of *N*-SuC NPs measured using the DLS technique was 66 ± 9 nm (Fig. 2C). The size of the *N*-SuC NPs observed by TEM was smaller than that obtained from the DLS technique. This difference may be due to the dehydration and shrinkage of NPs during the sample preparation process. Moreover, PDI of the *N*-SuC NPs was found to be 0.3 ± 0.1, and this smaller PDI value indicates that the *N*-SuC NPs have a narrow size distribution with a homogeneous dispersion. The zeta potential of *N*-SuC NPs was found to be +21 ± 5 mV, which can be attributed to the distribution of positively charged amine functionalities on the surface of *N*-SuC NPs (Fig. 2D). The viscoelastic properties of both *N*-SuC and N-SuC NPs solutions were investigated through dynamic rheological studies. Frequency sweep could reflect the interaction and structural characteristics of various components, and the changes in the storage module ($G'$) and loss modulus ($G''$) were studied as a function of frequency. Both $G'$ and $G''$ showed the dependence on frequency, and increased with the increase in frequency (Fig. 2E & F). The $G''$ value of *N*-SuC solution was higher than $G'$ at lower frequency indicating the viscous behavior, and at higher frequency, the order was slightly reversed with only a marginal difference between $G'$ and $G''$, and no crossover point within the tested range was observed indicating typical liquid-like solutions. In contrast, the *N*-SuC NPs solutions showed a higher $G'$ value almost throughout the frequency range, with a crossover point at the lowest frequency, suggesting the elastic behavior of the *N*-SuC NPs solutions. The presence of glycerol in the *N*-SuC NPs film forming solution weakens the inter or intramolecular force between the polymer chain, and thereby increases the elongation at break.

### 3.3. Characterization of N-SuC and N-SuC NPs films

Table 1 shows the mechanical properties of *N*-SuC and *N*-SuC NPs films, such as thickness, tensile strength, and elongation. *N*-SuC film was found to be thicker than the *N*-SuC NPs film. Clearly, *N*-SuC film demonstrated better mechanical properties than the *N*-SuC NPs film. For example, the *N*-SuC NPs film (3.3 ± 0.5 MPa) possessed a low tensile strength compared to the *N*-SuC film (10.3 ± 0.9 MPa). The presence of nanosized chitosan particles increased the electrostatic repulsion, thereby reducing the tensile strength of the *N*-SuC NPs film. The elongation of *N*-SuC and *N*-SuC NPs films was found to be 5.9 ± 0.8 and 9.3 ± 0.8%, respectively. The links formed as a result of the weak hydrogen bonds resulted in little flexibility.

**Table 1**
Thickness and mechanical properties of *N*-SuC and *N*-SuC NPs films. Four samples were analyzed in each case, and the values are given as mean ± standard deviation.

| Films | Thickness (μm) | Tensile strength (Mpa) | Elongation (%) |
|---|---|---|---|
| *N*-SuC | 79 ± 6 | 10.3 ± 0.9 | 5.9 ± 0.8 |
| *N*-SuC-NPs | 62 ± 6 | 3.3 ± 0.5 | 9.3 ± 0.8 |

One of the most important factors influencing the consumer attraction is the color and the appearance of the films. The photographic images of *N*-SuC and *N*-SuC NPs films showed clear, glossy and smooth appearance (Fig. 3A & B). But the visual appearance of *N*-SuC and *N*-SuC NPs films displayed well transparent slight yellow-colored films. Fig. 3C & D present the surface morphology of *N*-SuC and *N*-SuC NPs films, respectively. *N*-SuC film exhibited smooth, continuous and compact morphology without cracks or pores. *N*-SuC NPs film exhibited small spherical NPs with a mean particle diameter of 20 nm that are evenly distributed across the film structure.

Fig. 4 shows the AFM images and water contact angle measurements of *N*-SuC and *N*-SuC NPs films. AFM images of *N*-SuC film showed smooth surface with lower $R_a$ and $R_q$ values of 36 ± 4 and 46 ± 4 nm, respectively (Fig. 4A). *N*-SuC NPs film showed relatively rough surface, with high Ra and Rq values of 54 ± 6 and 73 ± 5 nm, respectively (Fig. 4B). The roughness differences between the *N*-SuC and *N*-SuC NPs films were consistent with the FESEM observations. A similar increase in the surface root mean square roughness has been reported for glycerol plasticized Tara gum film with chitosan NPs [40]. Hydrophilicity of *N*-SuC and *N*-SuC NPs film was investigated by water contact angle

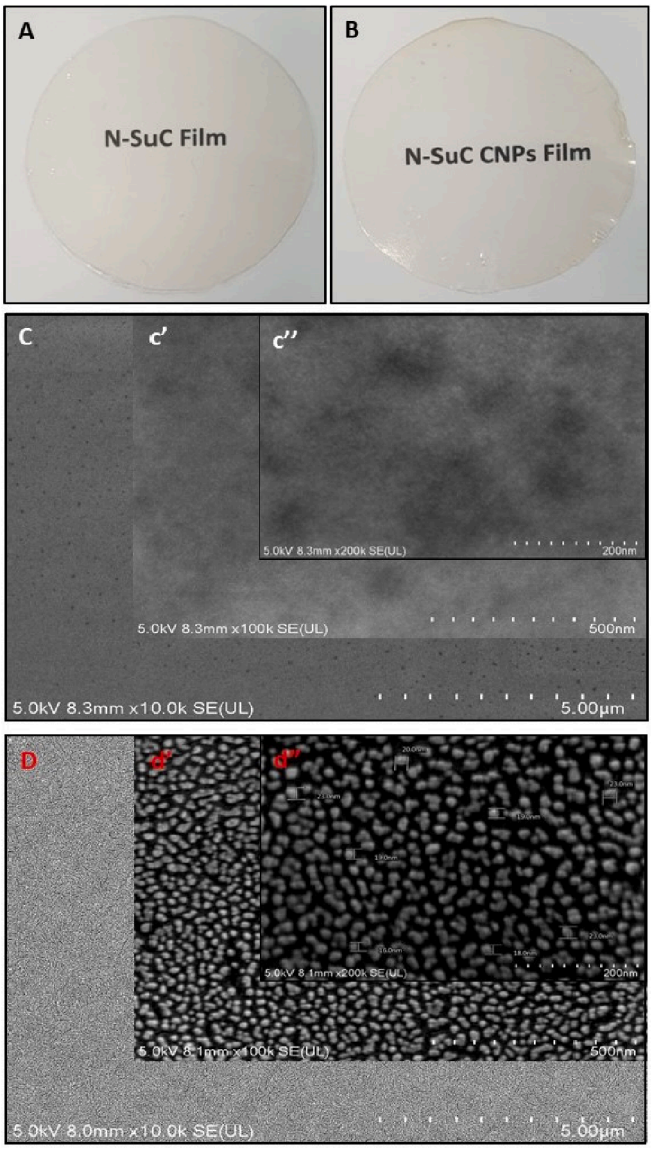


**Fig. 3.** Photograph images of (A) *N*-SuC film and (B) *N*-SuC NPs film; and FESEM images of (C) *N*-SuC film and (D) *N*-SuC NPs film. (insert in c' , c'' and d', d'' are different magnification images of corresponding films.).

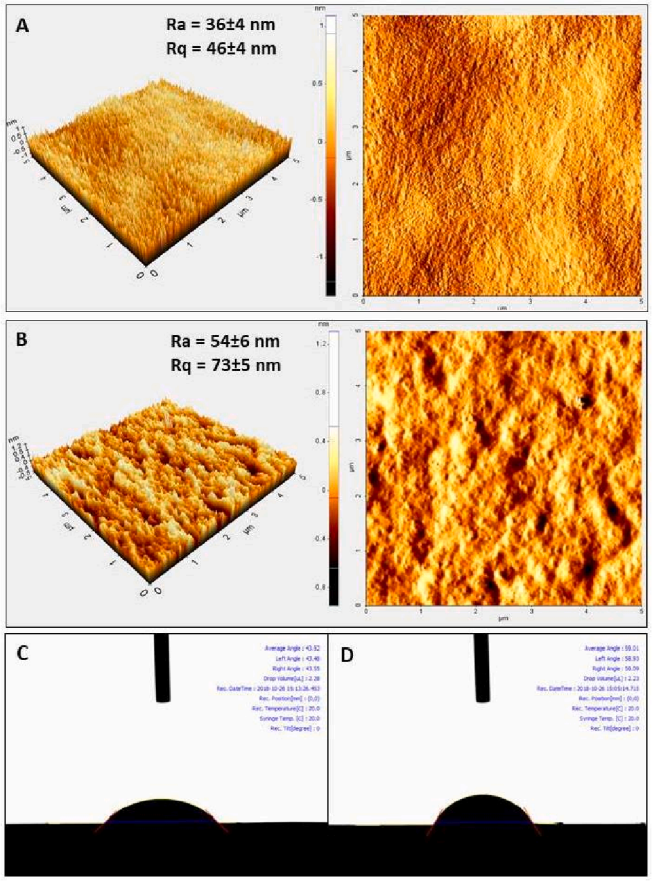


**Fig. 4.** AFM images of (A) *N*-SuC film, and (B) *N*-SuC NPs film; and water contact angle of sessile drops in (C) *N*-SuC film and (D) *N*-SuC NPs film.

measurements (Fig. 4C & D). The water contact angles of *N*-SuC and *N*-SuC NPs films were 38.6 ± 2.4° and 59.6 ± 3.3°, respectively. The pure chitosan film showed a high contact angle of 96.20°, which may be attributed to the hydrophobic backbone of the chitosan chains [28]. When compared to pure chitosan film, both *N*-SuC and *N*-SuC NPs films showed lower contact angle due to the presence of hydrophilic *N*-SuC chain. The hydrophilicity of *N*-SuC could be attributed to the introduction of polar carboxyl groups into the chitosan macromolecules during the formation of *N*-SuC. However, the increased surface roughness of *N*-SuC NPs film displayed relatively larger contact angle than *N*-SuC films, indicating that *N*-SuC NPs films are less hydrophilic than *N*-SuC films (Table 2).

### 3.4. Antibacterial activity of N-SuC and N-SuC NPs films

Microbila invasion is the main cause of the wound infections. Hence, the evaluation of antibacterial activity of the materials prior to the wound dressing applications is important. The antibacterial activity of *N*-SuC and *N*-SuC NPs films were evaluated against gram-positive (*S. aureus*) and gram-negative (*E. coli*) bacteria by determining the MIC and percentage inhibition ratio. *S. aureus* and *E. coli* are detrimental pathogens that can have serious clinical consequences in diabetic patients [41–43]. The MIC of *N*-SuC NPs film to inhibit the growth of *S. aureus* and *E. coli* bacteria were 6 mg/mL and < 8 mg/mL, respectively. The MIC of *N*-SuC film for both bacteria was greater than 8 mg/mL, indicating that there was no bacteriostatic effect. This low antibacterial effect of *N*-SuC film could attribute to the anionic nature of *N*-SuC. X. Niu et al. [44], also reported that the MIC of *N*-SuC was more than 5 mg/mL against *S. aureus* and *E. coli*.

Fig. 5A & B present the percentage inhibition ratio of *N*-SuC and *N*-SuC NPs films against *S. aureus* and *E. coli* bacteria. As seen in the figure, with increasing concentrations of *N*-SuC and *N*-SuC NPs films (from 0.5 to 8 mg/mL) the OD value decreased gradually, reflecting the augmentation of the growth inhibition. A comparison of OD values revealed stronger growth inhibition against *S. aureus* than *E. coli*. *N*-SuC NPs films at 6 and 8 mg/mL concentration showed 100% inhibition ratio against *S. aureus*. Generally, gram positive bacteria are more susceptible to antibacterial agents than the gram negative bacteria, since gram negative bacteria have less permeable lipid based outer membrane [45].

Biofilms consist of microbial communities embedded in a 3D extracellular matrix composed of a complex array of extracellular polymeric substances [46,47]. Formation of biofilms on chronic wounds hinders the healing process in the inflammatory state, and is responsible for ~80% of all chronic wound infections in humans [47,48]. Furthermore, the formation of biofilms in the wounds increases the resistance to antibiotics, reducing the phagocytosis during infection as well as the effectiveness of antimicrobial peptides belonging to the innate immune system [32,49]. Hence, the treatment of the wounds due to biofilms invasion becomes complicated, and the development of effective treatment methods to inhibit the biofilm formation is much needed. Fig. 5C & D shows the biofilms inhibition ratio of *N*-SuC and *N*-SuC NPs film elutes against *S. aureus* and *E. coli* bacteria. As seen in the figure, with the increase in the concentration of *N*-SuC and *N*-SuC NPs film elutes (from 0.5 to 8 mg/mL), the biofilm inhibition of *S. aureus* and *E. coli* bacteria also increases. For all the concentrations, *N*-SuC NPs film showed significantly high biofilm inhibition percentage than the *N*-SuC film ($p > 0.05$). Overall antibacterial results revealed that *N*-SuC and *N*-SuC NPs films possess excellent and sustained bacteriostatic action, and can be a good

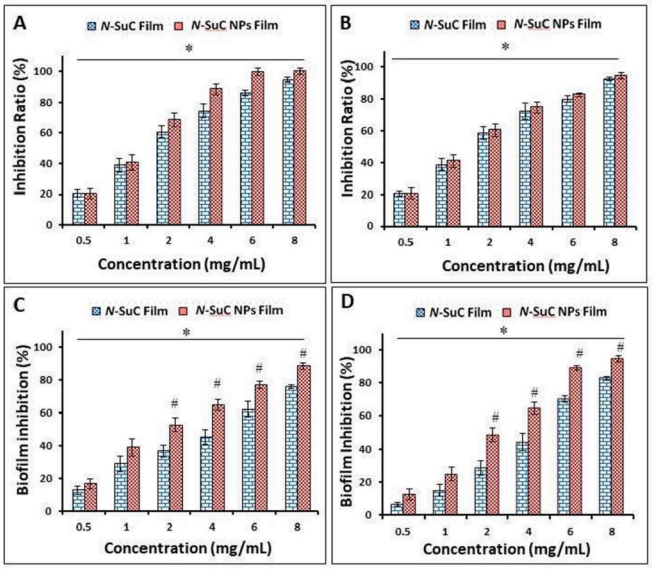


**Fig. 5.** Inhibition ratio for different concentrations of *N*-SuC and *N*-SuC NPs film against (A) *S. aureus* and (B) *E.coli* bacteria. Inhibition effects of *N*-SuC and *N*-SuC NPs film on biofilm of (C) *S. aureus* and (D) *E.coli*. Data are expressed as Mean ± *SE*, $n = 6$.*$p < 0.05$ *vs* control group (the biofilm without any treatment). # $p < 0.05$ for comparison between *N*-SuC and free *N*-SuC NPs film groups.

**Table 2**
Roughness parameters Ra and Rq obtained from AFM images and the contacts angles (CA) of water sessile drops. Four samples were analyzed in each case, and the values are given as mean ± standard deviation.

| Films | Ra (nm) | Rq (nm) | CA (°) |
|---|---|---|---|
| *N*-SuC | 36 ± 4 | 46 ± 4 | 38.6 ± 2.4 |
| *N*-SuC-NPs | 54 ± 6 | 73 ± 5 | 59.6 ± 3.3 |

candidate for chronic wound care and biofilm management.

### 3.5. Cytotoxicity assay of N-SuC and N-SuC NPs films

A good biomedical material should be nontoxic or only marginally toxic to the human body [50]. Before investigating the *in vivo* wound healing therapy, we evaluated the cytotoxicity of *N*-SuC and *N*-SuC NPs films on a mammalian cell (human dermal fibroblast cells, HDF) using the WST-1 assay. The cytotoxic potential is classified according to the percentage of cell viability (<50% toxic; 51–70% slightly toxic; >71% non-cytotoxic) [51]. The HDF cells cultured with the *N*-SuC and *N*-SuC NPs films elute at different concentrations for 48 h revealed no cytotoxic effects compared to the control (Fig. 6A). Interestingly, when compared to the control, *N*-SuC and *N*-SuC NPs films elute treated HDF cells showed significant ($p < 0.05$) cell viability between 400 and 800 and 200–800 μg/mL concentrations, respectively. The percentage viability of the cells treated with *N*-SuC and *N*-SuC NPs film elutes were higher than 100% even at high concentration (800 μg/mL), demonstrating the excellent proliferation effect of *N*-SuC and *N*-SuC NPs film elutes. As seen from the figures, both *N*-SuC and *N*-SuC NPs films elutes treated cells showed gradual increase in the percentage cell viability up to 600 μg/mL concentration. At 600 μg/mL concentration, the highest cell viability percentage was found to be 135.46% and 142.57%, respectively, for *N*-SuC and *N*-SuC NPs films elutes treated cells. Further increase in the concentration (>600 μg/mL) showed a decrease in the cell viability percentage. *N*-acetyl-d-glucosamine, a byproduct of chitosan degradation, may promote the fibroblast proliferation [52]. It has also been reported that *N*-SuC has the potential to promote the proliferation of L929cells to some extent, demonstrating its good biocompatibility for wound healing [16]. According to the cytotoxicity results, both *N*-SuC and *N*-SuC NPs films elutes were non-cytotoxic to HDF cells, indicating their good cytocompatibility for the use as a film.

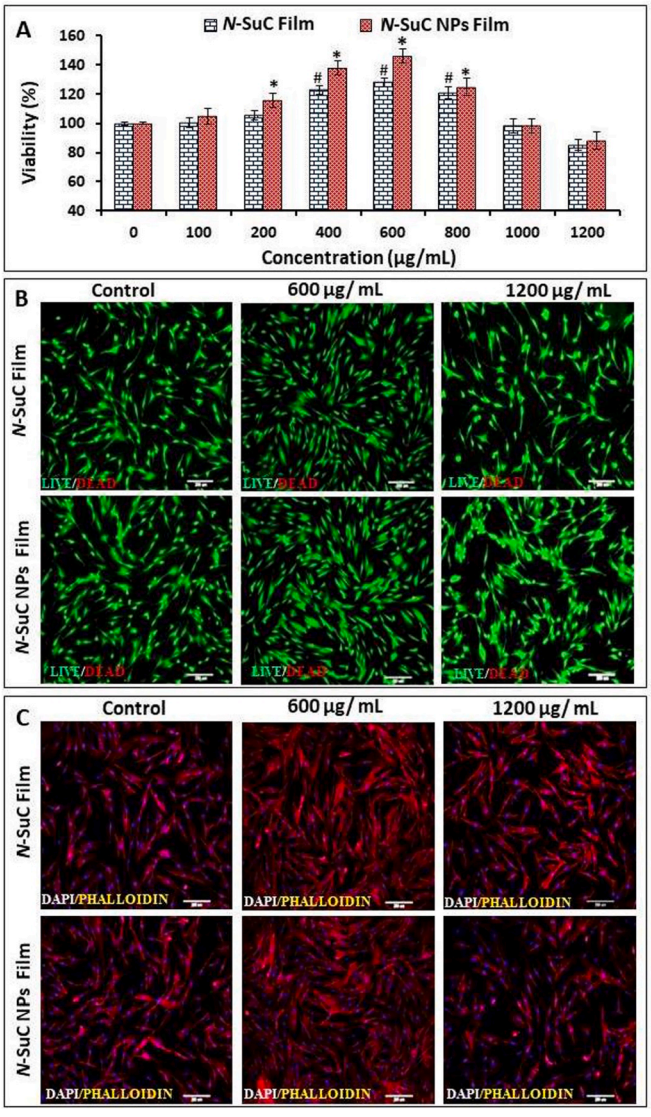


**Fig. 6.** Cytocompatible matrix of *N*-SuC and *N*-SuC NPs films (A) Cell viability of HDF cells after treatment with *N*-SuC and *N*-SuC NPs film elutes at different concentrations. The number sign and asterisks (#, *) indicates statistical significance of cell viability treated with the *N*-SuC and *N*-SuC NPs film elutes ($P < 0.05$); Fluorescent microscopic images of the cells after two days of the treatment with the elutes of *N*-SuC and *N*-SuC films using (B) live/dead assay, and (C) DAPI/Phallodine assay.

The cell viability and cell proliferation effect of *N*-SuC and *N*-SuC NPs films were further investigated by live/dead assay experiment (Fig. 6B). Elutes of *N*-SuC and *N*-SuC NPs films at the optimum (600 μg/mL) and at the highest (1200 μg/mL) concentrations treated cells were used for the live/dead assay. The DAPI and Phalloidin-TRIRC were used to stain the nucleus and actin cytoskeleton of live cells, respectively. The Phalloidin and DAPI stained images at 600 μg/mL of *N*-SuC and *N*-SuC NPs film elutes showed high cell proliferation and no cytotoxicity when compared to the control (Fig. 6C). In contrast, when treated with *N*-SuC and *N*-SuC NPs films elutes at 1200 g/mL, both *N*-SuC and *N*-SuC NPs films elutes showed little reduction in the cell proliferation effect when compared to the control. Taken together, the findings showed that the *N*-SuC NPs film elutes have no cytotoxicity and have the potential to increase the cell proliferation. As a result, it can be concluded that *N*-SuC NPs film is biologically compatible for *in vivo* wound healing.

### 3.6. In vitro wound healing activity of N-SuC and N-SuC NPs films

Cell growth and migration are critical features of the wound healing process during the tissue regeneration stage. The increased concentration of growth factors and cytokines caused by epithelial monolayer damage promotes the cell migration and proliferation [53]. This prompted us to investigate the wound healing capability of *N*-SuC and *N*-SuC NPs films. Elutes of *N*-SuC and *N*-SuC NPs films were used for the *in vitro* wound healing assay. The wound healing capability was evaluated by using a μ-Dish which was seeded to make confluent HDF monolayer with 500 μm cell free gap across the dish. Subsequently, the area of the cell free gap was measured upon treatment with 600 μg/mL *N*-SuC and *N*-SuC NPs elutes at 0, 12, 24 and 36 h of post treatment. Surprisingly, the *N*-SuC and *N*-SuC NPs film elutes treated HDF cells proliferate and decreased the cell free gap faster than the control (Fig. 7A). Moreover, the quantitative analysis of *N*-SuC ($p < 0.01$) and *N*-SuC NPs ($p < 0.001$) elute treatments after 24 and 36 h, revealed significant reduction of the cell free gap compared to the control. The percentage open wound area for the control, *N*-SuC and *N*-SuC NPs film elute after 24 h treatment was 78.86%, 58.25% and 35.25%, respectively, while after 36 h treatment the values were 42.52%, 15.25% and 5.25%, respectively (Fig. 7B). Nevertheless, *N*-SuC NPs film elute treatment was found to be significantly effective compared to the *N*-SuC film elute treatment ($p < 0.05$). Previous research found that, in addition to promoting the cell proliferation, *N*-SuC has the ability to improve the cell adhesion and maintain cell stability as the proliferation process progresses [54]. There are no previous reports on the direct effect of *N*-SuC NPs or *N*-SuC NPs film on the cell proliferation process. Few reports have demonstrated the cell migration and wound healing effects of chitosan NPs, chitosan NPs loaded hydrogel and chitosan NPs impregnated composite films [55–57]. However, our results reveal that elutes of *N*-SuC NPs film has the strongest capability of promoting HDF cell proliferation and migration *in vitro*.

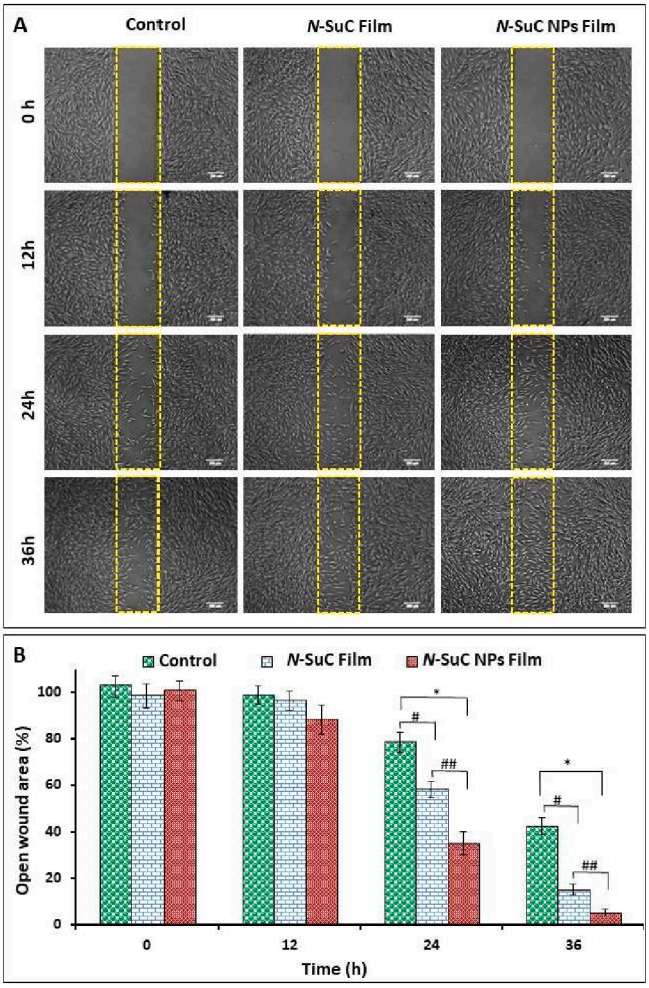


**Fig. 7.** (A) Photographic images of *in vitro* HDF cell migration after treatment *N*-SuC and *N*-SuC NPs film elutes (600 μg/mL), and (B) Quantitative analysis of the percentage open wound area. Data are expressed as Mean ± *SE*, $n = 6$.* $p < 0.05$ for comparison between control group and *N*-SuC NPs film groups, # $p < 0.05$ for comparison between control group and *N*-SuC film groups, $p < 0.05$ for comparison between *N*-SuC film group and *N*-SuC NPs film groups, Scale bar 200 μm.

### 3.7. *In vivo wound healing effect of N-SuC and N-SuC NPs film in Wister rats*

The wound healing potential of *N*-SuC and *N*-SuC NPs films was investigated by creating wound defects (8 mm diameter) on the dorsum of Wister rats. Fig. 8 shows the photographic images of the healing process of the wound sites after treatment with *N*-SuC and *N*-SuC NPs films. As seen in Fig. 9, the macroscopic wound closure percentage increased in the following order: *N*-SuC NPs film > *N*-SuC film > control. Initially (day 0), the surface of the wounds was covered with *N*-SuC and *N*-SuC NPs films of 8 mm diameter. On day 3, there was an obvious difference in the visible contraction of the wounds treated with the *N*-SuC NPs film compared to the control wounds treated with the *N*-SuC film. On day 7, both *N*-SuC and *N*-SuC NPs films treated wounds showed marked scab formation. The wound closure percentage after day 7 for the control, *N*-SuC film and *N*-SuC NPs film treatment were 65.34%, 72.48% and 84.21%, respectively (Fig. 9). On day 10, compared with the control and *N*-SuC film treated groups, the *N*-SuC NPs film treated wounds were significantly reduced in size, with almost complete wound closure. In addition, all wounds contracted from the edges, and a portion of the scab formation fell off. Scab formation was significantly reduced in the *N*-SuC film and *N*-SuC NPs film treated groups when compared to

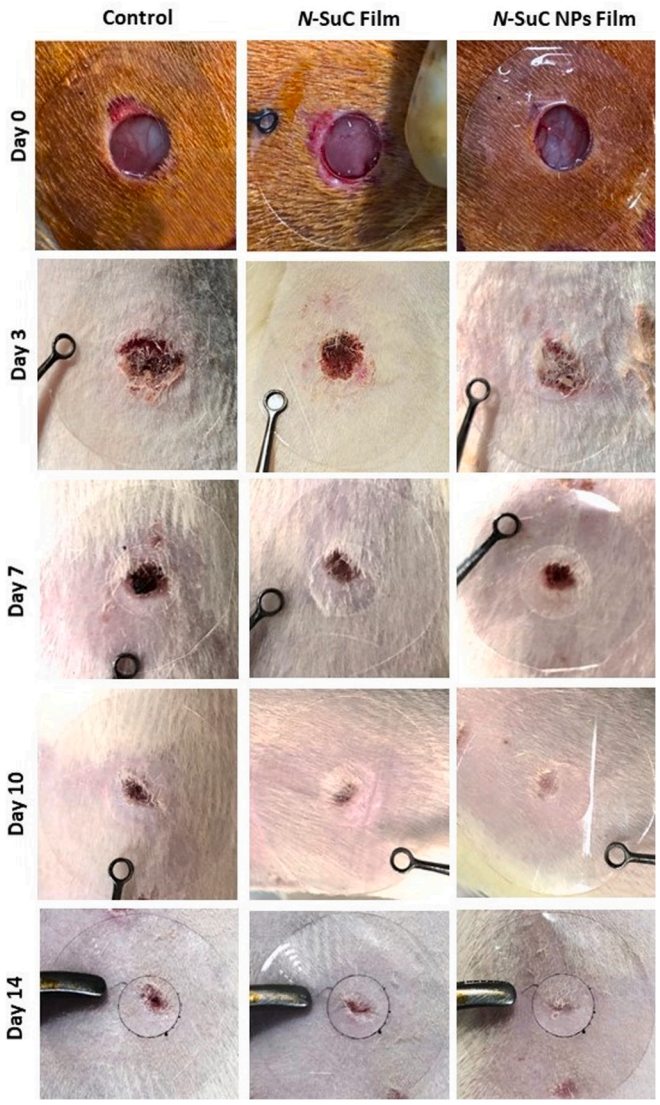


**Fig. 8.** *In vivo* photographs of the wounds treated with *N*-SuC and *N*-SuC NPs film, and control (not treated) at 0, 3, 7, 10, and 14 days of post-operation.

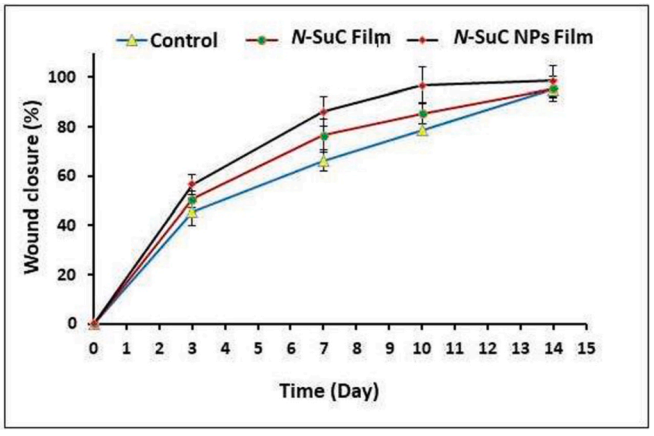


**Fig. 9.** Wound closure ratio of the control, *N*-SuC film, and *N*-SuC NPs film at different times. Data are expressed as Mean ± *SE*, $n = 12$.

the control group. The wound area in the *N*-SuC NPs film treated group was significantly shrunk with almost complete wound closure. On the 14$^{th}$ day, some scab formation could still be observed on the wound surface of the control group, whereas the *N*-SuC film treated group had only a minor scab formation on the wounds. Interestingly, the entire scab of the *N*-SuC NPs film treated group had fallen off and also the wound area became clean and pinkish in color, showing almost complete healing. These results indicate that *N*-SuC NPs film has a synergistic effect than the control and *N*-SuC film, thus promoting the wound healing and closure *in vivo*.

Wound healing process is often accompanied by inflammatory cell migration, neovascularization, fibroblast proliferation, epithelialization, and the production of extracellular matrix proteins [58]. After the chemical modification, the intermolecular and intramolecular H-bonds in the *N*-SuC were destroyed and more functional groups (carboxyl and amino) were exposed. The presence of many hydrophilic carboxyl groups conferred better water retention property to *N*-SuC allowing it to create a moist environment on the wound beds [59]. Also, the presence of many amino groups conferred better solubility and provided some favorable antibacterial effects. Furthermore, the adhesion of chitosan NPs to the biological surfaces is related to their high zeta potential [60]. Therefore, a high positive zeta potential of the synthesized *N*-SuC NPs ($+21 \pm 5$ mV) could contribute for the rapid adhesion of *N*-SuC NPs onto the wounds. In addition, a previous study found that covering a wound with a chitosan membrane accelerates healing due to its homeostatic effect, which was confirmed by increased epithelization and organized collagen deposition in the dermis [61]. In the case of *N*-SuC NPs film, the presence of polar carboxylate groups on the surface of the NPs lowers the interaction of the film with the red blood cells to a greater extent, thus minimizing the degree of disruption of the blood cells. From the results *in vivo* wound healing experiment, it is possible to conclude that *N*-SuC NPs film have a better wound closure and a shorter healing time.

Fig. 10 shows the histological evaluation of the wound sites after treatment with *N*-SuC and *N*-SuC NPs films. During the initial stage of the formation of new tissue, the fibroblasts migrate into the wounds and transformed into myofibroblast, leading to contraction and collagen deposition, forming granulation tissue [56]. In addition, the keratinous cells at the edge of the wounds are highly proliferating, covering the wound to form a new epidermis, which is the wound re-epithelialization [56]. The histological evaluation of the wound site on the 3$^{rd}$ day confirmed the inflammatory pattern of the healing process, when activated platelets secrete chemical mediators that stimulate vasodilatation, cellular proliferation, mainly neutrophils, monocytes, and macrophages [62]. As shown in figure ten, the H&E staining revealed that on the 3$^{rd}$ day, in the control group, large amount of inflammatory cells infiltration could observe in the wound sites. Furthermore, the granulation tissue layer structure remained loose, with only a few fibroblasts formed and arranged impacted. The *N*-SuC film did not show acute inflammatory reaction and a small number of inflammatory cells were observed in the wound sites. Moreover, *N*-SuC NPs film exhibited significant formation of fibroblast, granulation tissue and blood vessel at the wound sites. After treatment from day 3 to day 10, the wound was not completely closed and re-epithelialization was not completed in the control group. A scab formed in the center of the wound, the granulation tissue remained, and more neutrophil infiltration was visible around the border of epithelium. The wound sites treated with *N*-SuC and *N*-SuC NPs films had completed re-epithelialization, and a normal epidermis covered the wound area, with thicker and more dense collagen fibers. Some cutaneous annexes, such as sebaceous glands and hair follicles were formed in the center of the scar tissue. The healing process is usually confirmed by the presence of hair follicles as well as sweat and sebaceous gland [63]. The group treated with *N*-SuC NPs film showed complete epithelialization on the 14$^{th}$ day with regeneration of hair follicles and sebaceous glands. The epithelial thickness gradually increased until day 14 and is clearly visible. Fibroblasts and collagen were arranged orderly and only a very small amount of inflammation cells observed. Most of the granulation tissue and blood vessels subsided, tending to normal skin tissue. These histological data clearly evidenced that *N*-SuC NPs film accelerate the wound healing efficacy compared to the control and *N*-SuC film treated groups.

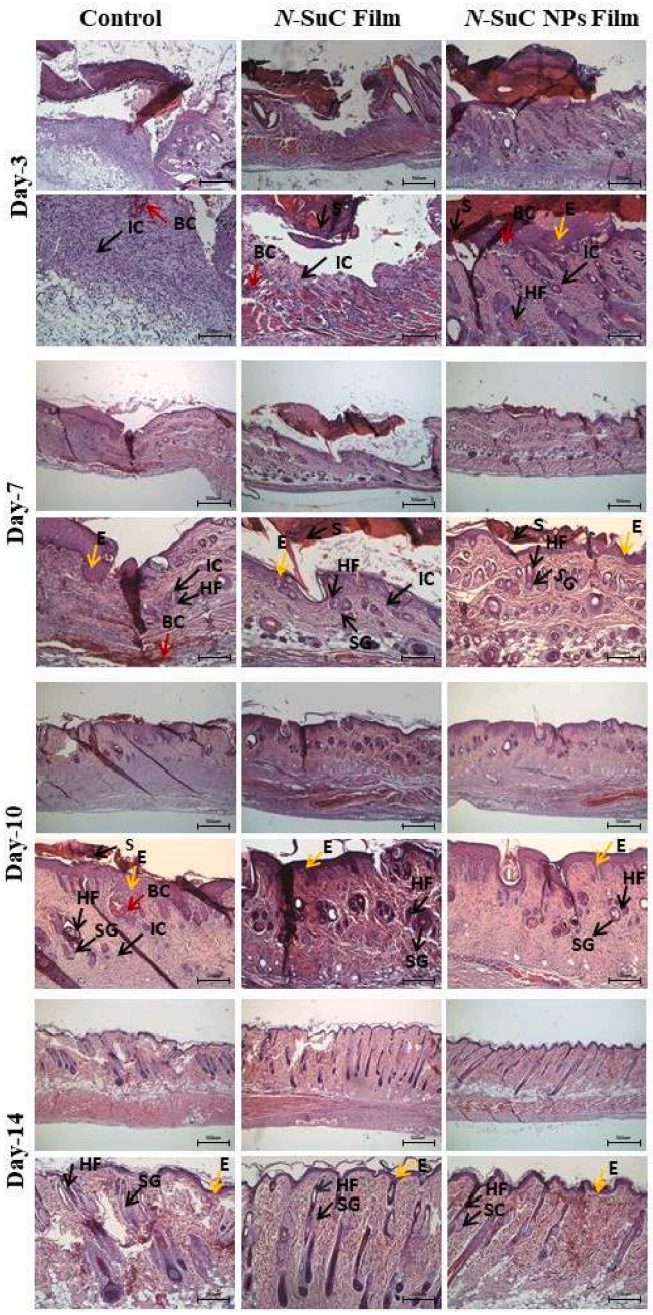


**Fig. 10.** Photomicrographs of the skin wound area determined *via* histological assay: Hematoxylin-eosin (H&E) staining was performed on paraffin block sections of the skin tissues of 3, 7, 10, and 14 days after initial wounding. (Magnification: ×40 and 100; E – epithelium, HF - hair follicles, SG - sebaceous gland, IC - inflammatory cells, S – Scarab, and BC - blood capillaries).

## 4. Conclusion

We successfully synthesized *N*-SuC and *N*-SuC NPs films and investigated the wound healing ability in Wistar rats for the first time. The synthesized *N*-SuC NPs and *N*-SuC NPs films demonstrated good mechanical properties, and are well characterized by various physiochemical methods such as $^{1}$H NMR, XRD, FTIR, FESEM, TEM, AFM *etc.*

The synthesized *N*-SuC NPs films showed good antibacterial activity against the gram-positive and gram-negative bacteria compared to *N*-SuC film. Both the *N*-SuC and *N*-SuC NPs film elutes showed remarkable HDF cell proliferation activity confirming their biocompatibility. *In vivo* wound healing ability on Wistar rat skin revealed that *N*-SuC NPs films significantly promote the granulation tissue formation and epithelialization, and shorten the healing time when compared to the control and *N*-SuC films. Our findings suggest that *N*-SuC NPs film have a high potential for use as a novel wound healing material.

## Declaration of competing interest

The authors declare that they have no known competing financial interests or personal relationships that could have appeared to influence the work reported in this paper.

## Acknowledgments

The authors thank the technicians from Leaders in Industry-University Cooperation (LINC), Dankook University for their technical assistance. The animal research team and technical staff in the Animal Research Facility Center at Faculty of Medicine, University of Ruhuna is acknowledged for their assistance in animal experiments.

## References

[1] F. Rezaie, M. Momeni-Moghaddam, H. Naderi-Meshkin, Regeneration and repair of skin wounds: various strategies for treatment, Int. J. Low Extrem. Wounds 18 (2019) 247–261, https://doi.org/10.1177/1534734619859214.
[2] A.M. Abdel-Mohsen, J. Frankova, R.M. Abdel-Rahman, A.A. Salem, N.M. Sahffie, I. Kubena, J. Jancar, Chitosan-glucan complex hollow fibers reinforced collagen wound dressing embedded with aloe vera. II. Multifunctional properties to promote cutaneous wound healing, Int. J. Pharm. 582 (2020), 119349, https://doi.org/10.1016/j.ijpharm.2020.119349.
[3] A. Khalil, M. Elmogy, M. Ghazal, C. Burns, A. El-Baz, Chronic wound healing assessment system based on different features modalities and non-negative matrix factorization (NMF) feature reduction, IEEE Access. 7 (2019) 80110–80121, https://doi.org/10.1109/ACCESS.2019.2923962.
[4] R.J. Boucek, Factors affecting wound healing, Otolaryngol. Clin. North Am. 17 (1984), https://doi.org/10.1016/S0030-6665(20)31963-0, 2430-264.
[5] T.A. Wilgus, S. Roy, J.C. McDaniel, Neutrophils and wound repair: positive actions and negative reactions, Adv. Wound Care 2 (2013) 379–388, https://doi.org/10.1089/wound.2012.0383.
[6] H.R. Shojania, M. Momeni-Moghaddam, S.-Ebrahim Hossini, M. Armin, J. Omrani Bidi, MicroRNA 155 downregulation by vitamin C-loaded human serum albumin nanoparticles during cutaneous wound healing in mice, Int. J. Low. Extrem. Wounds 18 (2019) 143–152, https://doi.org/10.1177/1534734619842975.
[7] A.S. Montaser, A.M. Abdel-Mohsen, M.A. Ramadan, A.A. Sleem, N.M. Sahffie, J. Jancar, A. Hebeish, Preparation and characterization of alginate/silver/nicotinamide nanocomposites for treating diabetic wounds, Int. J. Biol. Macromol. 92 (2016) 739–747, https://doi.org/10.1016/j.ijbiomac.2016.07.050.
[8] M.M.G. Fouda, A.M. Abdel-Mohsen, H. Ebaid, I. Hassan, J. Al-Tamimi, R.M. Abdel-Rahman, A. Metwalli, I. Alhazza, A. Rady, A. El-Faham, J. Jancar, Wound healing of different molecular weight of hyaluronan; in-vivo study, Int. J. Biol. Macromol. 89 (2016) 582–591, https://doi.org/10.1016/j.ijbiomac.2016.05.021.
[9] R.M. Abdel-Rahman, A.M. Abdel-Mohsen, R. Hrdina, L. Burgert, Z. Fohlerova, D. Pavliňák, O.N. Sayed, J. Jancar, Wound dressing based on chitosan/hyaluronan/nonwoven fabrics: preparation, characterization and medical applications, Int. J. Biol. Macromol. 89 (2016) 725–736, https://doi.org/10.1016/j.ijbiomac.2016.04.087.
[10] R.M. Abdel-Rahman, R. Hrdina, A.M. Abdel-Mohsen, M.M.G. Fouda, A.Y. Soliman, F.K. Mohamed, K. Mohsin, T.D. Pinto, Chitin and chitosan from Brazilian Atlantic Coast: isolation, characterization and antibacterial activity, Int. J. Biol. Macromol. 80 (2015) 107–120, https://doi.org/10.1016/j.ijbiomac.2015.06.027.
[11] L.I.F. Moura, A.M.A. Dias, E. Carvalho, H.C. de Sousa, Recent advances on the development of wound dressings for diabetic foot ulcer treatment - a review, Acta Biomater. 9 (2013) 7093–7114, https://doi.org/10.1016/j.actbio.2013.03.033.
[12] X. Huang, Y. Sun, J. Nie, W. Lu, L. Yang, Z. Zhang, H. Yin, Z. Wang, Q. Hu, Using absorbable chitosan hemostatic sponges as a promising surgical dressing, Int. J. Biol. Macromol. 75 (2015) 322–329, https://doi.org/10.1016/j.ijbiomac.2015.01.049.
[13] B. Evranos, D. Aycan, N. Alemdar, Production of ciprofloxacin loaded chitosan/gelatin/bone ash wound dressing with improved mechanical properties, Carbohydr. Polym. 222 (2019), 115007, https://doi.org/10.1016/j.carbpol.2019.115007.
[14] C. Qin, H. Li, Q. Xiao, Y. Liu, J. Zhu, Y. Du, Water-solubility of chitosan and its antimicrobial activity, Carbohydr. Polym. 63 (2006) 367–374, https://doi.org/10.1016/j.carbpol.2005.09.023.
[15] V. Patrulea, V. Ostafe, G. Borchard, O. Jordan, Chitosan as a starting material for wound healing applications, Eur. J. Pharm. Biopharm. 97 (2015) 417–426, https://doi.org/10.1016/j.ejpb.2015.08.004.
[16] F. Tang, L. Lv, F. Lu, B. Rong, Z. Li, B. Lu, K. Yu, J. Liu, F. Dai, D. Wu, G. Lan, Preparation and characterization of N-chitosan as a wound healing accelerator, Int. J. Biol. Macromol. 93 (2016) 1295–1303, https://doi.org/10.1016/j.ijbiomac.2016.09.101.
[17] S. Sun, A. Wang, Adsorption properties of carboxymethyl-chitosan and cross-linked carboxymethyl-chitosan resin with Cu(II) as template, Sep. Purif. Technol. 49 (2006) 197–204, https://doi.org/10.1016/j.seppur.2005.09.013.
[18] S. Sun, A. Wang, Adsorption properties of N-succinyl-chitosan and cross-linked N-succinyl-chitosan resin with Pb(II) as template ions, Sep. Purif. Technol. 51 (2006) 409–415, https://doi.org/10.1016/j.seppur.2006.03.004.
[19] C. Yan, D. Chen, J. Gu, H. Hu, X. Zhao, M. Qiao, Preparation of N-succinyl-chitosan and their physical-chemical properties as a novel excipient, Yakugaku Zasshi 126 (2006) 789–793, https://doi.org/10.1248/yakushi.126.789.
[20] Y.A. Skorik, A.S. Kritchenkov, Y.E. Moskalenko, A.A. Golyshev, S.V. Raik, A. K. Whaley, L.V. Vasina, Dmitry L. Sonin, Synthesis of N-succinyl- and N-glutaryl-chitosan derivatives and their antioxidant, antiplatelet, and anticoagulant activity, Carbohydr. Polym. 166 (2017) 166–172, https://doi.org/10.1016/j.carbpol.2017.02.097.
[21] P. Calvo, R. Lopez, J.L. Vila-Jato, M.J. Alonso, Novel hydrophilic chitosan-polyethylene oxide nanoparticles as protein carriers, J. Appl. Polym. Sci. 63 (1997) 125–132, https://doi.org/10.1002/(sici)1097-4628(19970103)63:1<125::aid-app13>3.0.co;2-4.
[22] C. Yan, D. Chen, J. Gu, J. Qin, Nanoparticles of 5-fluorouracil (5-FU) loaded N-succinyl-chitosan (Suc-Chi) for cancer chemotherapy: preparation, characterization - in-vitro drug release and anti-tumour activity, J. Pharm. Pharmacol. 58 (2006) 1177–1181, https://doi.org/10.1211/jpp.58.9.0003.
[23] Q. Zhu, Y. Zhou, M. Guan, X. Zhou, S. Yang, Y. Liu, W. Chen, C. Zhang, Z. Yuan, C. Liu, A. Zhu, X. Zhang, Low-density lipoprotein-coupled N-succinyl chitosan nanoparticles co-delivering siRNA and doxorubicin for hepatocyte-targeted therapy, Biomaterials 35 (2014) 5965–5976, https://doi.org/10.1016/j.biomaterials.2014.03.088.
[24] Z. Hou, J. Han, C. Zhan, C. Zhou, Q. Hu, Q. Zhang, Synthesis and evaluation of N-succinyl-chitosan nanoparticles toward local hydroxycamptothecin delivery, Carbohydr. Polym. 81 (2010) 765–768, https://doi.org/10.1016/j.carbpol.2010.02.009.
[25] M.R. de Moura, M.V. Lorevice, L.H.C. Mattoso, V. Zucolotto, Highly stable, edible cellulose films incorporating chitosan nanoparticles, J. Food Sci. 76 (2011) N25–N29, https://doi.org/10.1111/j.1750-3841.2010.02013.x.
[26] R.A. Shapi'i, S.H. Othman, N. Nordin, R.Kadir Basha, M.Nazli Naim, Antimicrobial properties of starch films incorporated with chitosan nanoparticles: In vitro and in vivo evaluation, Carbohydr. Polym. 230 (2020), 115602, https://doi.org/10.1016/j.carbpol.2019.115602.
[27] P.R. Chang, R. Jian, J. Yu, X. Ma, Fabrication and characterization of chitosan nanoparticles/plasticised-starch composites, Food Chem. 120 (2010) 736–740, https://doi.org/10.1016/j.foodchem.2009.11.002.
[28] S.F. Hosseini, M. Rezaei, M. Zandi, F. Farahmandghavi, Development of bioactive fish gelatin/chitosan nanoparticles composite films with antimicrobial properties, Food Chem. 194 (2016) 1266–1274, https://doi.org/10.1016/j.foodchem.2015.09.004.
[29] L. Perez-Alvarez, L. Ruiz-Rubio, J.L. Vilas-Vilela, Determining the deacetylation degree of chitosan: opportunities to learn instrumental techniques, J. Chem. Educ. 95 (2018) 1022–1028, https://doi.org/10.1021/acs.jchemed.7b00902.
[30] E.K.W. Toh, H.Y. Chen, Y.L. Lo, S.J. Huang, L.F. Wang, Succinated chitosan as a gene carrier for improved chitosan solubility and gene transfection, Nanomedicine 7 (2011) 174–183, https://doi.org/10.1016/j.nano.2010.07.007.
[31] J. Palacio, Y. Monsalve, F. Ramírez-Rodríguez, B. López, Study of encapsulation of polyphenols on succinyl-chitosan nanoparticles, J. Drug Deliv. Sci. Technol. 57 (2020), 101610, https://doi.org/10.1016/j.jddst.2020.101610.
[32] A. Asli, E. Brouillette, C. Ster, M.G. Ghinet, R. Brzezinski, P. Lacasse, M. Jacques, F. Malouin, Antibiofilm and antibacterial effects of specific chitosan molecules on Staphylococcus aureus isolates associated with bovine mastitis, PLoS ONE 12 (2017), e0176988, https://doi.org/10.1371/journal.pone.0176988.
[33] E.A. Kamoun, N-succinyl chitosan–dialdehyde starch hybrid hydrogels for biomedical applications, J. Adv. Res. 7 (2016) 69–77, https://doi.org/10.1016/j.jare.2015.02.002.
[34] P. Mukhopadhyay, S. Maity, S. Mandal, A.S. Chakraborti, A.K. Prajapati, P. P. Kundu, Preparation, characterization and in vivo evaluation of pH sensitive, safe quercetin-succinylated chitosan-alginate core-shell-corona nanoparticle for diabetes treatment, Carbohydr. Polym. 182 (2018) 42–51, https://doi.org/10.1016/j.carbpol.2017.10.098.
[35] S.H.S. Dananjaya, S.L. Edirisinghe, N.T. Thu Thao, R. Saravana Kumar, H.M.S. M. Wijerathna, A.Y. Mudiyanselage, M. De Zoysa, D. Choi, Succinyl chitosan gold nanocomposite: preparation, characterization, in vitro and in vivo anticandidal activity, Int. J. Biol. Macromol. 165 (2020) 63–70, https://doi.org/10.1016/j.ijbiomac.2020.09.126.
[36] A. Li, Q. Xue, Y. Ye, P. Gong, M. Deng, B. Jiang, Study on TEMPO-mediated oxidation of N-succinyl chitosan and the water retention property, Molecules 25 (2020) 4698, https://doi.org/10.3390/molecules25204698.
[37] J.S. Lee, H. Nah, H.J. Moon, S.J. Lee, D.N. Heo, I.K. Kwon, Controllable delivery system: a temperature and pH-responsive injectable hydrogel from succinylated

chitosan, Appl. Surf. Sci. 528 (2020), 146812, https://doi.org/10.1016/j.apsusc.2020.146812.
[38] X. Qing, G. He, Z. Liu, Y. Yin, W. Cai, L. Fan, P. Fardim, Preparation and properties of polyvinyl alcohol/N-succinyl chitosan/ lincomycin composite antibacterial hydrogels for wound dressing, Carbohydr. Polym. 261 (2021), 117875, https://doi.org/10.1016/j.carbpol.2021.117875.
[39] S. Hassani, A. Laouini, C.Charcosset Fessi, Preparation of chitosan-TPP nanoparticles using microengineered membranes - effect of parameters and encapsulation of tacrine, Colloids Surf. A Physicochem. Eng. Asp. 482 (2015) 34–43, https://doi.org/10.1016/j.colsurfa.2015.04.006.
[40] J. Antoniou, F. Liu, H. Majeed, F. Zhon, Characterization of tara gum edible films incorporated with bulk chitosan and chitosan nanoparticles: a comparative study, Food Hydrocoll. 44 (2015) 309–319, https://doi.org/10.1016/j.foodhyd.2014.09.023.
[41] Z.A. Kanafani, W.M. Kourany, V.G. Fowler, D.P. Levine, G.A. Vigliani, M. Campion, D.E. Katz, G.R. Corey, H.W. Boucher, Clinical characteristics and outcomes of diabetic patients with Staphylococcus aureus bacteremia and endocarditis, Eur. J. Clin. Microbiol. Infect. Dis. 28 (2009) 1477–1482, https://doi.org/10.1007/s10096-009-0808-3.
[42] K.M. Todorovic, I. Eminovic, N.I. Mehmedinovic, M. Ibrisimovic, Insulin acts as stimulatory agent in diabetes-related Escherichia coli pathogenesis, Int. J. Diabetes Clin. Res. 5 (2018), 098, https://doi.org/10.23937/2377-3634/1410098.
[43] A.M. Abdel-Mohsen, J. Jancar, D. Massoud, Z. Fohlerova, H. Elhadidy, Z. Spotz, A. Hebeish, Novel chitin/chitosan-glucan wound dressing: isolation, characterization, antibacterial activity and wound healing properties, Int. J. Pharm. 510 (2016) 86–99, https://doi.org/10.1016/j.ijpharm.2016.06.003.
[44] X. Niu, L. Zhu, L. Xi, L. Guo, H. Wang, An antimicrobial agent prepared by N-succinyl chitosan immobilized lysozyme and its application in strawberry preservation, Food Control 108 (2020), 106829, https://doi.org/10.1016/j.foodcont.2019.106829.
[45] D. Hu, H. Wang, L. Wang, Physical properties and antibacterial activity of quaternized chitosan/carboxymethyl cellulose blend films, Food Sci. Technol. 65 (2016) 398–405, https://doi.org/10.1016/j.lwt.2015.08.033.
[46] P.J. Alves, R.T. Barreto, B.M. Barrois, L.G. Gryson, S. Meaume, S.J. Monstrey, Update on the role of antiseptics in the management of chronic wounds with critical colonisation and/or biofilm, Int. Wound J. 18 (2021) 342–358, https://doi.org/10.1111/iwj.13537.
[47] S.L. Percival, C. Vuotto, G. Donelli, B.A. Lipsky, Biofilms and wounds: an identification algorithm and potential treatment options, Adv. Wound Care 4 (2015) 389–397, https://doi.org/10.1089/wound.2014.0574.
[48] C.H. Thomson, Biofilms: do they affect wound healing? Int. Wound J. 8 (2011) 63–67, https://doi.org/10.1111/j.1742-481X.2010.00749.x.
[49] N. Hoiby, T. Bjarnsholt, M. Givskov, S. Molin, O. Ciofu, Antibiotic resistance of bacterial biofilms, Int. J. Antimicrob. Agents 35 (2010) 322–332, https://doi.org/10.1016/j.ijantimicag.2009.12.011.
[50] X. Zhou, L. Xu, J. Xu, J. Wu, T.B. Kirk, D.M.W. Xue, Construction of a high-efficiency drug and gene co-delivery system for cancer therapy from a pH-sensitive supramolecular inclusion between oligoethylenimine- graft-β-cyclodextrin and hyperbranched polyglycerol derivative, ACS Appl. Mater. Interfaces 10 (2018) 35812–35829, https://doi.org/10.1021/acsami.8b14517.
[51] H.M. Avila, S. Schwarz, E.M. Feldmann, A. Mantas, A. von Bomhard, P. Gatenholm, N. Rotter, Biocompatibility evaluation of densified bacterial nanocellulose hydrogel as an implant material for auricular cartilage regeneration, Appl. Microbiol. Biotechnol. 98 (2014) 7423–7435, https://doi.org/10.1007/s00253-014-5819-z.
[52] R. Jayakumar, M. Prabaharan, P.T.S. Kumar, S.V. Nair, H. Tamura, Biomaterials based on chitin and chitosan in wound dressing applications, Biotechnol. Adv. 29 (2011) 322–337, https://doi.org/10.1016/j.biotechadv.2011.01.005.
[53] S. Shyna, A. Shanti Krishna, P.D. Nair, L.V. Thomas, A nonadherent chitosan-polyvinyl alcohol absorbent wound dressing prepared via controlled freeze-dry technology, Int. J. Biol. Macromol. 150 (2020) 129–140, https://doi.org/10.1016/j.ijbiomac.2020.01.292.
[54] S. Bashir, Y.Y. Teo, S. Ramesh, K. Ramesh, A.A. Khan, N-succinyl chitosan preparation, characterization, properties and biomedical applications: a state of the art review, Rev. Chem. Eng. 31 (2015) 563–597, https://doi.org/10.1515/revce-2015-0016.
[55] A. Choudhary, V. Kant, B.L. Jangir, V.G. Joshi, Quercetin loaded chitosan tripolyphosphate nanoparticles accelerated cutaneous wound healing in Wistar rats, Eur. J. Pharmacol. 880 (2020), 173172, https://doi.org/10.1016/j.ejphar.2020.173172.
[56] T. Wang, Y. Zheng, Y. Shen, Y. Shi, F. Li, C. Su, L. Zhao, Chitosan nanoparticles loaded hydrogels promote skin wound healing through the modulation of reactive oxygen species, Artif. Cells nanomedBiotechnol. 46 (2018) 138–149, https://doi.org/10.1080/21691401.2017.1415212.
[57] M. Sun, Q. Xie, X. Cai, Z. Liu, Y. Wang, X. Dong, Y. Xu, Preparation and characterization of epigallocatechin gallate, ascorbic acid, gelatin, chitosan nanoparticles and their beneficial effect on wound healing of diabetic mice, Int. J. Biol. Macromol. 148 (2020) 777–784, https://doi.org/10.1016/j.ijbiomac.2020.01.198.
[58] S. Schreml, R.M. Szeimies, L. Prantl, M. Landthaler, P. Babilas, Wound healing in the 21st century, J. Am. Acad. Dermatol. 63 (5) (2010) 866–881, https://doi.org/10.1016/j.jaad.2009.10.048.
[59] X. Wang, D. Zhang, J. Wang, R. Tang, B. Wei, Q. Jiang, Succinyl pullulan-crosslinked carboxymethyl chitosan sponges for potential wound dressing, Int. J. Polym. Mater. 66 (2016) 61–70, https://doi.org/10.1080/00914037.2016.1182912.
[60] A.L.P. Neves, C.C. Milioli, L. Muller, H.G. Riella, N.C. Kuhnen, H.K. Stulzer, Factorial design as tools in chitosan nanoparticles development by ionic gelation technique, Colloids Surf. A Physicochem. Eng. Asp. 445 (2014) 34–39 (10.1016%2Fj.colsurfa.2013.12.058).
[61] F.L. Mi, S.S. Shyu, Y.B. Wu, S.T. Lee, J.Y. Shyong, R.N. Huang, Fabrication and characterization of a sponge-like asymmetric chitosan membrane as a wound dressing, Biomaterials 22 (2001) 165–173, https://doi.org/10.1016/s0142-9612(00)00167-8.
[62] M. Shafique, M. Sohail, M.U. Minhas, T. Khaliq, M. Kousar, S. Khan, Z. Hussain, A. Mahmood, M. Abbasi, H.C. Aziz, S.A. Shah, Bio-functional hydrogel membranes loaded with chitosan nanoparticles for accelerated wound healing, Int. J. Biol. Macromol. 170 (2021) 207–221, https://doi.org/10.1016/j.ijbiomac.2020.12.157.
[63] M.C. Ribeiro, V.L.R. Correa, F.K.Lopes da Silva, A.A. Casas, Angelica de Lima das Chagas, L.Paula de Oliveira, M.P. Miguel, D.G.A. Diniz, A.C. Amaral, L.Borges de Menezes, Wound healing treatment using insulin within polymeric nanoparticles in the diabetes animal model, Eur. J. Pharm. Sci. 150 (2020), 105330, https://doi.org/10.1016/j.ejps.2020.105330.